Vol. 48 — N° 2 06 24 p. 393 – 410

GEOSTANDARDS and GEOANALYTICAL RESEARCH

Molybdenite Reference Materials for *In Situ* LA-ICP-MS/MS Re-Os Geochronology

Renée **Tamblyn** (1, 2)*, Sarah **Gilbert** (3), Stijn **Glorie** (1, 4), Carl **Spandler** (1), Alexander **Simpson** (1, 4), Martin **Hand** (1, 4), Derrick **Hasterok** (1, 4), Bryant **Ware** (5) and Svetlana **Tessalina** (5)

(1) Department of Earth Sciences, University of Adelaide 5005, South Australia, Australia
(2) Current address: Institute for Geology, University of Bern, Baltzerstrasse 1 + 3, Bern 3012, Switzerland
(3) Adelaide Microscopy, University of Adelaide 5005, South Australia, Australia
(4) Mineral Exploration Cooperative Research Centre, University of Adelaide 5005, Australia
(5) John de Laeter Centre, Curtin University, Bentley, 6845, Western Australia, Australia
* Corresponding author. e-mail: renee.tamblyn@unibe.ch

Re-Os isotope-dilution geochronology has been widely used to date the timing of molybdenite, pyrite and chalcopyrite formation across a variety of geological settings. However, *in situ* methods have been impeded by the isobaric interference of ^{187}Re on ^{187}Os. *In situ* Re-Os geochronology using LA-ICP-MS/MS has been shown to be a useful technique to chemically separate Os from Re, as Os reacts with CH_4 to create higher-mass reaction products, which can then be measured with minimised interference of ^{187}Re. However, application of the method requires matrix-matched primary reference materials, e.g., age-homogenous molybdenite amenable to laser ablation. Here, we characterise and present two new molybdenite mineral reference materials for *in situ* Re-Os geochronology by LA-ICP-MS/MS, verified by ID-TIMS Re-Os measurements. We also present case studies from molybdenite samples with varying Re mass fractions and Re-Os age mapping. The method provides accurate and precise age data, with excellent precision for high Re samples. The benefits of the LA-ICP-MS/MS approach include: (1) simple sample preparation, (2) rapid data acquisition, (3) targeting of specific textural domains including growth zones and (4) the ability to simultaneously collect trace elements used to link the timing and conditions of ore-formation.

Keywords: Re-Os, molybdenite, LA-ICP-MS/MS, reaction gas.

Received 28 Aug 23 – Accepted 14 Feb 24

Re-Os geochronology is an important tool for understanding the timing of metalliferous ore formation and the depositional ages of organic-rich sediments (e.g., Hirt 1963, Stein *et al.* 2001, Selby and Creaser 2004). Rhenium is a strongly chalcophile element that can be concentrated in hydrothermally-derived sulfides such as pyrite (FeS_2), chalcopyrite ($CuFeS_2$) and, most notably, molybdenite (MoS_2, Stein *et al.* 2002, Barton *et al.* 2019). Dating molybdenite with the Re-Os isotope system is demonstrably robust, as molybdenite generally does not incorporate significant Os during crystallisation, and can remain unaffected by later high-grade metamorphism, deformation and hydrothermal fluid flow events (Stein *et al.* 2001, Bingen and Stein 2003, Barra *et al.* 2017). Consequently, a large number of studies have used Re-Os geochronology to constrain the timing of mineralisation in a variety of ore deposits and petroleum systems (e.g., Stein *et al.* 2001, Bingen and Stein 2003, Barra *et al.* 2017, Sai *et al.* 2020). These studies relied on isotope dilution thermal ionisation mass spectrometry (ID-TIMS) based measurements on chemically separated Re and Os aliquots (e.g., Selby and Creaser 2001a, b, Selby *et al.* 2009, Barra *et al.* 2005, Hou *et al.* 2006, Stein 2014, Feely *et al.* 2020).

Attempts to measure Re-Os isotopes via laser ablation-inductively coupled plasma-mass spectrometry (LA-ICP-MS) have proven difficult, principally because of the large (> 90%) corrections necessary to deconvolve the isobaric

doi: 10.1111/ggr.12550

interference of ^{187}Re on ^{187}Os. Additional to this problem, authors have suggested that the Re-Os system in molybdenite is susceptible to resetting, where parent and daughter isotopes exhibit contrasting mobilities leading to age heterogeneities (e.g., Košler *et al.* 2003, Stein *et al.* 2003, Selby and Creaser 2004, Zimmerman *et al.* 2022). This apparent isotopic decoupling behaviour can result in large age variations within crystals, perhaps detectable by *in situ* LA-ICP-MS. The isotope dilution method circumvents this behaviour because large grains are crushed and homogenised with the assumption that at some scale, the analysed sample is isotopically closed (Selby and Creaser 2004). However, a disadvantage of grain-scale homogenisation is the destruction of any isotopic record related to growth zoning, recrystallisation and sub-grain development during later events.

LA-ICP-MS/MS has proved a fruitful avenue to chemically distinguish isobaric interferences between Re and Os with the use of methane as a reaction gas (Håkansson 2019, Hogmalm *et al.* 2019). In the LA-ICP-MS/MS set-up, a reaction cell (also referred to as the "collision/reaction cell") is housed between two quadrupole mass analysers. The first quadrupole acts as a mass filter, allowing only one preselected isotope (or *m/z* ratio) to enter the reaction cell at a time, which then reacts with the gas to form product ions with higher mass. The second quadrupole is set to the mass of the product ion, enabling chemical separation of isobaric interferences. This technique is used to measure isotope ratios from beta decay isotope systems, where the daughter isotope reacts efficiently with the reaction gas, but the parent does not, for example ^{87}Rb-^{87}Sr (Zack and Hogmalm 2016, Hogmalm *et al.* 2017, Redaa *et al.* 2021) and ^{176}Lu-^{176}Hf (Simpson *et al.* 2021, 2022, Tamblyn *et al.* 2022). The set-up is also useful for the removal of interferences in alpha decay systems, e.g., the removal of common lead in the U-Pb system (Gilbert and Glorie 2020). It has been demonstrated that for the Re-Os system, ^{187}Os reacts with CH_4 to produce $OsCH_2^+$ with a mass of 201 (i.e., +14 mass-shift), while ^{187}Re is less reactive (e.g., Hogmalm *et al.* 2019). Hogmalm *et al.* (2019) used a molybdenite mineral nano-powder as the primary reference material, which has the potential limitation that its ablation characteristics differ from natural molybdenite mineral grains (e.g., Redaa *et al.* 2021), and precludes evaluation of within-grain Re-Os isotopic disequilibrium in reference materials (Hogmalm *et al.* 2019). *In situ* Re-Os isotopic measurement via LA-ICP-MS/MS may benefit from the development of matrix-matched reference material crystals with sufficient Re and Os mass fractions, well-characterised and homogenous Re-Os isotope ratios, and sufficiently large crystals for easy mounting and ablation.

We have characterised two natural molybdenite mineral samples from Queensland, Australia and Quebec, Canada, by both LA-ICP-MS/MS and ID-TIMS, and demonstrate they can be reliably used as primary reference materials (RMs) for *in situ* Re-Os geochronology. Using these primary RMs, we explore the advantages and limitations of the *in situ* Re-Os method by presenting Re-Os age data, including Re-Os age maps, for molybdenite samples with variable Re mass fractions (ranging between 0.1 and 5100 μg g^{-1}). We demonstrate the uncertainties on the *in situ* Re-Os weighted mean ages from Re-rich molybdenite can approach those of ID-TIMS analysis. The main advantages of the *in situ* method are: (1) the speed of data acquisition, (2) the spatial and textural resolution of Re-Os sampling within mineral grains, and (3) the ability to collect trace element data simultaneously that provides petrogenetic information that can be directly tied to the age data.

Samples

Merlin deposit, Queensland, Australia

The Merlin deposit is located within the Cloncurry district of the Mt. Isa Inlier, Queensland, Australia. It is the highest-grade Mo-Re deposit known in the world and is hosted by a metasedimentary rock package comprising phyllite, carbonaceous slate and calc-silicate rocks (Brown *et al.* 2010, Babo *et al.* 2017). Mo-Re mineralisation occurs in two styles, (1) infill of matrix-supported hydrothermal breccias and (2) stylolitic veins and disseminations (Babo *et al.* 2017). The matrix infill molybdenite gives a Re-Os ID-TIMS age of 1535 ± 6 Ma (Table 1; Duncan *et al.* 2013, Babo *et al.* 2017), however vein and disseminated molybdenite taken from drill core give Re-Os ID-TIMS ages of 1521 ± 6 Ma to 1529 ± 6 Ma (Babo *et al.* 2017). Minor Mo-Re mineralisation hosted in carbonate veins gives a Re-Os ID-TIMS age of 1503 ± 5 Ma (Babo *et al.* 2017). Duncan *et al.* (2013) also report one older Re-Os age (1559 ± 5 Ma) from the deposit, but the petrological context and geological significance of this molybdenite age is not clear (Babo *et al.* 2017).

Two molybdenite samples with pre-existing Re-Os ID-TIMS ages (Babo *et al.* 2017) were chosen for this study: sample MDQ0252 taken at 466.25 m depth from drill core MDQ0252 and sample MDQ0221 taken at and 473.8 m depth from drill core MDQ0221 (Table 1). Sample MDQ0252 is a partially stylolitic molybdenite vein, 5 mm in diameter, and was used as a primary reference material in this study. Sample MDQ0221 consists of smaller (0.5 mm

Table 1.
Samples measured in this study

Sample name	Location	Mineral	Previous geochronology	Method	References	Re mass fraction (μg g^{-1}) (this study)	Re-Os LA-ICP-MS/MS weighted mean age (this study)	Re-Os ID TIMS age (this study)	Os/Re ratio for RMs (this study)
MDC0252	Merlin deposit, Queensland, Australia	Molybdenite	1520 ± 6 Ma	Molybdenite Re-Os ID TIMS	Babo *et al.* (2017)	65–5100	1518 ± 4 Ma	1520 ± 4 Ma	0.025649 ± 0.000105
MDC0221	Merlin deposit, Queensland, Australia	Molybdenite	1523 ± 6 Ma	Molybdenite Re-Os ID TIMS	Babo *et al.* (2017)	60–1300	1516 ± 6 Ma		
Q-MolyHill	Moly Hill, Quebec, Canada	Molybdenite	2750 ± 27 Ma; 2624 ± 5; 2646 ± 120 Ma	Molybdenite Re-Os ID TIMS	Birck *et al.* (1997), Suzuki *et al.* (1993)	5–60	2620 ± 10 Ma	2623 ± 6 Ma	0.044699 ± 0.000166
NT-Jinka	Molyhil, Northern Territory, Australia	Molybdenite	1701.6 ± 4.8 Ma; 1720 ± 5.9 Ma	Hornblende Ar-Ar SH; Molybdenite Re-Os ID TIMS	Reno and Fraser (2021), Cross (2009)	0.1–15	1710 ± 23 Ma		
M15581	Moonta, South Australia, Australia	Molybdenite	1599 ± 6 Ma; 1574 ± 6 Ma	Molybdenite Re-Os ID TIMS	Skirrow *et al.* (2007)	50–320	1575 ± 12 Ma		

in diameter) molybdenite veins. An additional molybdenite sample (MDQ0120) was chosen for age and trace element mapping.

Moly Hill, Quebec, Canada

The Moly Hill deposit is located in La Motte within the Abitibi belt, Quebec, Canada. Molybdenite is hosted in quartz veins/pegmatites within the Preissac pluton, a late-Archaean muscovite monzogranite intrusion (Sabina 2003). Crystallisation of the Preissac pluton has been dated to 2681–2660 Ma by U-Pb and Sm-Nd geochronology of monazite and titanite (Ducharme *et al.* 1997). Molybdenite from the pluton was dated by ID-TIMS Re-Os geochronology at 2766–2526 Ma (range of three ages) and 2750 ± 27 Ma, recalculated from Suzuki *et al.* (1993) and Birck *et al.* (1997) by Košler *et al.* (2003) with the updated Re decay constant of 1.6668 ± 0.0034 × 10^{-11} (Table 1). One molybdenite sample (named Q-MolyHill) hosted with coarse-grained quartz was obtained from a commercial mineral specimen supplier. The sample consists of a single euhedral freestanding crystal of 1.25 cm in diameter.

Jinka Moly, Northern Territory, Australia

The Molyhil skarn deposit is located in the Jinka area of the Aileron Province of central Australia, ~ 225 km to the northeast of Alice Springs (Barraclough 1979). The Mo-W mineralisation occurs at the contact between altered metacarbonates (Deep Bore Metamorphics) and granite (Marshall Granite), where the intruding granite provided the hydrothermal fluids for skarn formation. U-Pb zircon age data indicates the granite crystallised between ~ 1732–1720 Ma (Kositcin *et al.* 2018). Previous molybdenite ID-TIMS Re-Os analysis gave an age of 1720 ± 8 Ma (Table 1; Huston *et al.* 2021) and Ar-Ar step heating of hornblende from the skarn gave an age of 1701.6 ± 4.8 Ma (Reno and Fraser 2021).

A sample of molybdenite was obtained from the Molyhil deposit. In order to clearly distinguish this sample from Moly Hill in Quebec, the sample is named NT-Jinka. Molybdenite from Jinka forms grains up to 2.5 cm in length and together with chalcopyrite overprints a magnetite-quartz-apatite-amphibole skarn assemblage.

Moonta-Wallaroo, South Australia, Australia

The Moonta-Wallaroo district is located in the southern Olympic Cu-Au province in the eastern Gawler Craton (South Australia) and is characterised by iron oxide Cu-Au mineralisation (Ruano *et al.* 2002, Bockmann *et al.* 2022). Molybdenite occurs as a minor phase in Cu-Au-bearing veins within metasediments and felsic magmatic rocks of the Wallaroo Group (Skirrow *et al.* 2007). Re-Os ID-TIMS geochronology of molybdenite from geophysically contrasting areas in the Moonta-Wallaroo give ages of 1599 ± 6 Ma and 1574 ± 6 Ma (Table 1; Skirrow *et al.* 2007).

A sample (M15581) of pure coarse-grained (> 3 cm) molybdenite from the Yelta Mine locality (Table 1) was obtained from the Tate Memorial Museum at the University of Adelaide. Yelta is located within the same geophysical domain as the younger of the two ID-TIMS molybdenite ages.

Methods

Sample preparation

All samples were mounted as rock blocks or mineral grains in 25-mm epoxy disks, and polished using 3-µm diamond paste. Care was taken to polish each molybdenite sample on a separate piece of sandpaper or cloth, to avoid smearing and cross-contamination of the soft molybdenite grains. Grains were optically examined under reflected light for inclusions.

In situ LA-ICP-MS/MS spot analyses

The Re-Os measurements were undertaken using a RESOlution-LR 193 nm excimer laser ablation system (Applied Spectra), with a S155 sample chamber (Laurin Technic), coupled to an Agilent 8900 ICP-MS/MS, housed at Adelaide Microscopy, the University of Adelaide. A squid mixing device (Laurin Technic) was used to smooth the signals from the laser ablation system. Measurements were conducted across three sessions, with an initial session to determine optimal gas flow rates for efficient reaction of Os. CH_4 was used as the reaction gas, after Hogmalm *et al.* (2019, 99.999% purity), in the first session at a flow rate of 0.223 ml min^{-1}, and in the second two sessions at a flow rate of 0.388 ml min^{-1} (20 and 35% on Mass Flow Controller 4, respectively). In the first session, He was added at a flow rate of 7 ml min^{-1} to test the effect on sensitivity and reaction rates. A reaction product ion scan was run to confirm mass 201 ($^{187}Os^{12}C^{2}H_2^{+}$) as the optimal reacted mass of ^{187}Os (Hogmalm *et al.* 2019), referred to herein as $^{187+14}Os$. Samples that are characterised for Re mass fractions (synthetic glass NIST SRM 610 and sulfide RM STDGL3, Jochum *et al.* 2011, Danyushevsky *et al.* 2011), and Os (synthetic sulfide reference material NiS3, Gilbert *et al.* 2013), were analysed to optimise reaction rates in the reaction cell for $^{187+14}Os$, while supressing reaction rates for interference $^{187+14}Re$. N_2 was added (at 3.5 ml min^{-1}) to the carrier gas after the sample chamber to increase sensitivity (Hu *et al.* 2008). The ICP-MS/MS was first tuned in the absence of the CH_4 reaction gas (no-gas mode) to minimise oxide interferences and to optimise N_2 and Ar gas flow rates for a robust plasma, and then tuned with CH_4 reaction gas to maximise sensitivity for the Os reaction products using the CH_4 reaction gas mixture.

Molybdenite crystals were ablated with a fluence of 3.0 J cm^{-2} at a repetition rate of 5 Hz, and with laser spot diameters of 30, 43, 67, 100 and 120 µm. The following isotopes for geochronological calculations were measured, with mass shifts in brackets: ^{185}Re, $^{(185+14)}Re$, $^{187}Os+Re$, $^{(187+14)}Os$ (which contains some reacted ^{187}Re), ^{189}Os and $^{(189+14)}Os$ (Table 2). A number of additional masses were measured to monitor inclusions and trace elements in the molybdenite (Table 2). Analyses included 30 s of background followed by 30 to 40 s of ablation. Dwell times for the measured masses are in Table 2.

All LA-ICP-MS/MS spot analysis data processing was completed using the software LADR (Norris and Danyushevsky 2018), to correct for gas background, monitor for down-hole fractionation and calibrate for instrument mass bias and drift. We note that $^{187}Re/^{187}Os$ down-hole fractionation in molybdenite was not detected in this study, regardless of the spot size used (e.g., Figure 1). Due to the potential for unreacted ^{187}Os and ^{187}Re at mass 187, ^{185}Re was measured as a proxy and ^{187}Re calculated assuming natural abundance. In our observations, ~ 1.3–2.5% of the ^{187}Re reacts with CH_4 and, therefore, an

Table 2.
Dwell times for measured masses

Element	Q1 → Q2 (mass → mass shift)	Dwell time (ms) Sessions 1, 2, 3
Al	27	2
S	34	2
Fe	57	2
Ni	60	2
Cu	65	2
Zn	66	2
Nb	93	2
Mo	95	2
Ag	109	2
Sn	118	2
Te	125	2
Ta	181	2
W	182	2
Re	185	20
Re	185 → 199	80, 50, 50
Re (+Os)	187	50
Os (+Re)	187 → 201	200, 200, 180
Os	189 → 203	80, 80, 150
Pb	208	2
Bi	209	2

→ indicates a mass shift by reaction with CH_4.

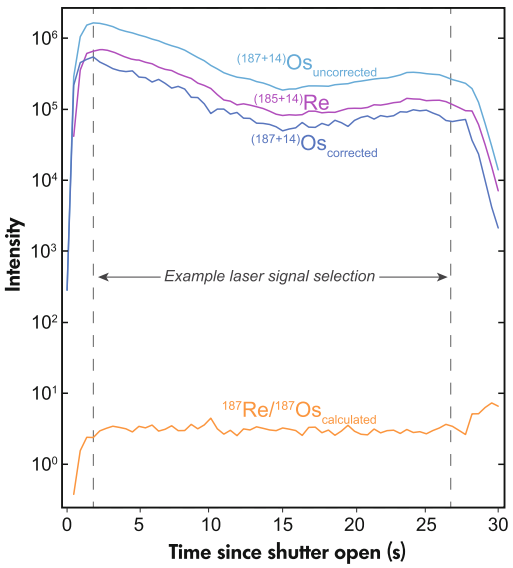

Figure 1. Example LA-ICP-MS/MS ablation signal from molybdenite sample MDQ0252 from the Merlin deposit, prior to processing in LADR (Norris and Danyushevsky 2018), analysed with a 43 µm spot size, and containing ~ 450 µg g^{-1} Re. $^{(187+14)}Os_{corrected}$ refers to the counts of $^{(187+14)}Os$ corrected for the ^{187}Re which also reacts with CH_4. The molybdenite contains variable ^{185}Re but has a homogenous $^{187}Re/^{187}Os$ ratio with no detectable down-hole fractionation. Common Os (measured as ^{189}Os) was not detected.

interference correction was carried out by calculating the amount of $^{187+14}Re$ present in each analysis from the measured $^{185+14}Re$ counts by assuming natural abundance and subtracting this from the raw $^{187+14}Os$ counts. The interference correction is carried out prior to calculating the average ratio for each analysis and normalisation to the primary reference material. The session run with 0.223 ml min^{-1} CH_4 and 7 ml min^{-1} He has a Re reaction rates of 1.3%, and the sessions run with 0.388 ml min^{-1} CH_4 have Re reaction rates between 2 and 2.5% (online supporting information Figure S1). Therefore, He may have the effect of reducing the Re interference, with the caveat that it also reduces sensitivity on the reaction products. The mass fractionation for interference corrections was corrected by measuring $^{187}Re/^{185}Re$ in NIST610, which contains negligible Os (Jochum *et al.* 2011, Hogmalm *et al.* 2019), the resulting mass bias is calculated as 0.988. As Re mass fractions are high in molybdenite, this interference correction can be significant (up to 75%) for low Re or young samples, currently limiting the applicability of the method to high Re samples (> 10 µg g^{-1}, depending on age), or old samples, which have accumulated sufficient radiogenic Os (> *ca.* 200 Ma, depending on Re mass fraction). Work is on-going with other reaction gases to further suppress Re reaction rates. Common Os was monitored on masses ^{189}Os and $^{189+14}Os$, although was not detected in significant mass fractions in any measured molybdenite in this study. Ages were calculated in IsoplotR (Vermeesch 2018) from $^{187}Re/^{187+14}Os$ using the ^{187}Re decay constant on 1.6668 ± 0.0034 × 10^{-11}, the uncertainty on the decay constant is propagated into age uncertainties (Košler *et al.* 2003). Prior to this study, there were no natural Re-Os mineral grains available as primary RMs for laser-ablation Re-Os geochronology. We have characterised the molybdenite sample MDQ0252 (see further information below) with a previously measured $^{187}Os/^{187}Re$ ratio of 0.0256 ± 0.0001024 (Babo *et al.* 2017) to use as a primary reference material. The $^{187}Os/^{187}Re$ ratio calculated in this study from ID-TIMS and used for all isotopic calibrations was 0.025649 ± 0.000105, refer to the *Results* section for further details. For trace elements, the reference materials used were the synthetic sulfide reference material NiS3 (Gilbert *et al.* 2013) and the synthetic glass reference material NIST SRM 610 (Jochum *et al.* 2011). Molybdenum was used as the internal standard element for molybdenite, at 59.94% *m/m*. As the reference material used was matrix-matched to the molybdenite samples, no further correction factors were required.

LA-ICP-MS/MS mapping methods

LA-ICP-MS/MS maps were collected to verify homogeneity of the $^{187}Re/^{187}Os$ ratio in the primary reference material and to explore the potential applications of isotopic ratio mapping. Rhenium, Os and trace elements were acquired simultaneously using the dwell times listed in Table 2. Laser and mass spectrometer settings were the same as those for spot analyses, except that the squid mixing device was removed to improve response time and spatial resolution, and the raster spot size and scan speed were 20 µm and 10 µm s^{-1} respectively. The raw $^{(187+14)}Os$ counts per second (cps) data were corrected for the ^{187}Re interference, using the measured $^{(185+14)}Re$ as described above. These data were then imported to Iolite3 to correct for instrument drift and mass bias (Paton *et al.* 2011), to produce corrected $^{187}Re/^{(187+14)}Os$ ratios. Subsequently Re-Os ages were calculated using the ^{187}Re decay constant of 1.6668 ± 0.0034 × 10^{-11}. Age maps and trace element maps were then generated using Laser Map Explorer (in-house software, Hasterok *et al.* in prep.). The maps were filtered (Table 3) to identify the molybdenite grains and remove contamination from epoxy at the edges and holes in the grain. For both maps, noise reduction was applied using

Table 3.
Filter parameters for age maps and associated statistical estimates

Analyte	MDQ0120		MDQ0252	
	Filter range	Percent removed	Filter range	Percent removed
Mo (cps)	2×10^8 to 8×10^8	25.4	0.5×10^8 to 4.8×10^8	6.7
Al (cps)	$< 1 \times 10^7$	17.3	$< 1 \times 10^7$	5.5
Date (Ma)	< 3500 Ma	0.4	< 3500 Ma	< 0.1

three filters: (1) ^{95}Mo cps $< 0.5 \times 10^8$ (to ensure only moly data is shown), (2) ^{27}Al cps $> 1 \times 10^7$ (to remove significant inclusions), and (3) Re-Os age > 3500 Ma (to remove extreme noise; > 2× the age of the mineral). The age filter removed < 0.1% and < 0.4% for MDQ0252 and MDQ0120, respectively. The Mo filter mostly removes empty zones around the margins of the map, the Al filter removed epoxy contamination around the holes and the date filter removed date estimates more than three standard deviations from the mean.

ID-TIMS analyses

The two primary reference material candidates (MDQ0252 and Q-MolyHill) were further characterised for Re-Os isotopic analysis using ID-TIMS at the John de Laeter Centre (JdLC), Curtin University, Western Australia.

The isotope dilution technique was used in conjunction with the Carius tube method, to digest the sample material and equilibrate the sample-spike (Shirey and Walker 1995). To measure the abundance of ^{187}Re and ^{187}Os in molybdenite by isotope dilution technique, we used a mixed ^{185}Re-^{188}Os-^{190}Os double spike, following the approach described in Markey *et al.* (2003, 2007). For this study, the JdLC spike was designed with a ^{188}Os/^{190}Os ratio near unity to provide for a more precise determination of the fractionation correction, following the University of Alberta Radiogenic Isotope Facility (RIF) methodology. The ^{187}Os-^{190}Os abundance in the double spike was calibrated against the ammonium hexachloro-osmate AB2, which was prepared and calibrated at RIF (Selby and Creaser 2001). For the initial calibration of our spike, we simultaneously determined the isotopic composition and the concentration of the double spike, by measuring separately double spike and the spike-standard mixture. The ^{185}Re abundance in mixed spike solution was calibrated against a gravimetric Re standard solution made from 99.999% Re metal and shows a reproducibility better than 0.4% 2*s* (n = 5).

Multiple aliquots of each molybdenite sample were weighed (~ 10 to 60 mg) and transferred directly into cleaned Carius tubes. A carefully weighed amount of aforementioned mixed double spike was then added to each Carius tube. Inverse *aqua regia* (1 ml concentrated, PTFE-distilled hydrochloric acid and 3 ml concentrated, PTFE-distilled purged nitric acid) was subsequently added to the Carius tubes and frozen to prevent loss of volatile Os. Once each tube had been sealed, the samples were digested overnight in an oven at 220 °C. After complete digestion, Os was separated from the inverse *aqua regia* sample solution by solvent extraction (Cohen and Waters 1996), with final purification of the Os achieved via micro-distillation (Brick *et al.* 1997). Rhenium separation was achieved using anion exchange chromatography.

The purified Os was loaded onto platinum filaments with a NaOH-Ba(OH)$_2$ activator solution and the Os isotopic measurements were obtained using negative TIMS on a Thermo Scientific Triton™. Osmium isotope determinations were conducted either using a secondary electron multiplier detector in peak jumping mode, or on Faraday collectors in static mode. Long-term 'instrument reproducibility' on the Triton™ was monitored through the measurement of the AB2 Os reference material (University of Alberta) during each measurement session, yielding a ^{187}Os/^{188}Os isotope ratio of 0.10682 ± 0.00018 (n = 5, 2*s*), consistent with the 0.10684 ± 0.00004 ^{187}Os/^{188}Os isotope ratio reported by Selby and Creaser (2003). The Re isotopic compositions and mass fractions were determined in solution via ICP-MS on a Thermo Scientific ELEMENT XR™. The mean of multiple measurements of a natural Re standard solution returned an ^{185}Re/^{187}Re isotopic ratio of 0.59285 ± 0.00042 (n = 106, 2*s*), with the uncertainty being just outside the natural ^{185}Re/^{187}Re isotopic ratio of 0.5974 (Gramlich *et al.* 1973). Subsequently, a minor fractionation correction was applied.

Error propagation on individual measurements includes uncertainties associated with the calibration of the spike, mass spectrometer measurements, and blank corrections. Due to the high Re and ^{187}Os mass fractions for these molybdenite samples, analytical blanks are essentially insignificant for age calculations. Procedural blank values for Os were 0.4 ± 0.1 pg (n = 2) and 1.7 ± 0.4 pg for Re. The ^{187}Os/^{188}Os ratios for the blank were 0.38 ± 0.08.

The 'Henderson molybdenite' reference material (Henderson RM) was used to monitor inter-laboratory agreement and clean laboratory chemical purification procedures. Three aliquots ranging from weights of ~ 30–60 mg were processed using the identical procedure described above

for the unknowns. The Henderson RM results yielded Re-Os model ages of 27.764 ± 0.125 Ma, 27.509 ± 0.126 Ma, and 28.142 ± 0.123 Ma; with two analyses being within uncertainty of the literature value of 27.656 ± 0.022 Ma (95% confidence; Markey *et al.* 2007) and the third being outside the literature uncertainty.

Results

In situ LA-ICP-MS/MS spot analyses

All obtained data have been pooled and presented from across three measurement sessions (online supporting information Table S1). The presented uncertainties are 2 standard error of the means and calculated ages include the uncertainty on the ^{187}Re decay constant. For dates where the MSWD is > 1, i.e., greater than expected for a single population of *N*, the presented uncertainties include overdispersion (Vermeesch 2018). The primary reference material for the Re-Os isotopic measurements was molybdenite sample MDQ0252 from Merlin. Analyses of MDQ0252 show variable Re and Os mass fractions, but consistent ^{187}Os/^{185}Re ratios and therefore ages (e.g., Figures 1 and 2a). Rhenium mass fractions range between 65 and 5100 μg g^{-1}. The weighted mean age of the LA-ICP-MS/MS ages for MDQ0252 (i.e., as the primary reference material) is 1518 ± 4 Ma, (Figure 2a, *n* = 71, MSWD = 0.87), which excludes one analysis as an outlier. The small uncertainty on the weighted mean age is due to limited dispersion in the single-point data.

A separate molybdenite sample from Merlin (MDQ0221), with Re mass fractions between 60 and 1300 μg g^{-1} and an ID-TIMS age of 1523 ± 6 Ma (Babo *et al.* 2017), was run as a secondary reference material. Across the three sessions MDQ0221 returned a weighted mean Re-Os age of 1516 ± 6 Ma (Figure 2b, *n* = 70, MSWD = 0.77), with two analyses excluded as outliers.

Molybdenite from Moly Hill in Quebec (Q-MolyHill) was measured across two measurement sessions and returned an *in situ* Re-Os age of 2620 ± 10 Ma (*n* = 62, MSWD = 0.54), with Re mass fractions of 5–60 μg g^{-1}. Two analyses were excluded from the age calculation as outliers (Figure 2c).

NT-Jinka molybdenite was measured in one session, and the calculated ages show more significant dispersion compared with other samples (Figure 2d). The weighted mean of the ages gives 1710 ± 23 Ma (*n* = 45, MSWD = 2.88), with five analyses excluded as outliers (as statistically calculated by the program IsoplotR, Vermeesch *et al.* 2018). The dispersed ages tail out to *ca.* 1300 and *ca.* 2100 Ma (Figure 2d). Rhenium mass fractions in the molybdenite are low, and range between 0.1–15 μg g^{-1}.

Molybdenite from the Moonta-Wallaroo district (M15581) was analysed in one session and gives a weighted mean age of 1575 ± 12 Ma (Figure 2e, *n* = 20, MSWD = 0.48). The Re mass fraction ranges between 50 and 320 μg g^{-1}.

LA-ICP-MS/MS mapping results

LA-ICP-MS/MS mapping of two samples of molybdenite from Merlin is presented in Figure 3. Sample MDQ0252 is largely homogenous in Re-Os age, despite the strong Re zoning in the molybdenite. Minor apparent age differences largely occur at holes or cracks in the crystal, and/or areas with very low Re. Hence, when such areas are avoided, the crystal can be regarded as homogenous for the purpose of laser ablation dating. A vein of molybdenite from another sample in the Merlin deposit (MDQ0120) shows minor age zoning that correlates with enrichment in trace elements, but low Re mass fractions.

ID-TIMS

Results of ID-TIMS analyses of samples MDQ0252 and Q-Molyhill are presented in Table 4 and Figure 4. Six aliquots of MDQ0252 were analysed, and show dispersed ^{187}Os/^{187}Re ratios and ages, ranging from 1501 ± 6 Ma to 1527 ± 11 Ma (Figure 4a). The dispersion in age correlates to Re mass fractions, with higher Re aliquots (ranging from 1043 to 1617 μg g^{-1}) producing progressively younger ages (Figure 4c). When a weighted mean is calculated excluding one very Re rich (> 1300 μg g^{-1}) outlier (as determined by the program IsoplotR, Vermeesch *et al.* 2018), the ^{187}Os/^{187}Re ratio is 0.025649 ± 0.000041 or ± 0.000105 if 'overdispersion' is considered (MSWD = 3.3, Vermeesch *et al.* 2018), corresponding to a weighted mean of the Re-Os ages of 1520 ± 4 Ma, including the uncertainty on the Re decay constant (Figure 4, *n* = 5, MSWD = 1.3). This ^{187}Re/^{187}Os ratio was used as the primary RM for LA-ICP-MS/MS analyses.

Five aliquots of Q-MolyHill yield slightly dispersed ^{187}Os/^{187}Re ratios that are also inversely correlated with Re mass fraction. However, the variation in Re mass fraction is relatively low (between 44 to 51 μg g^{-1}) and a statistically acceptable weighed mean ^{187}Os/^{187}Re ratio of 0.044699 ± 0.00006 or 0.00017 if 'overdispersion' is considered

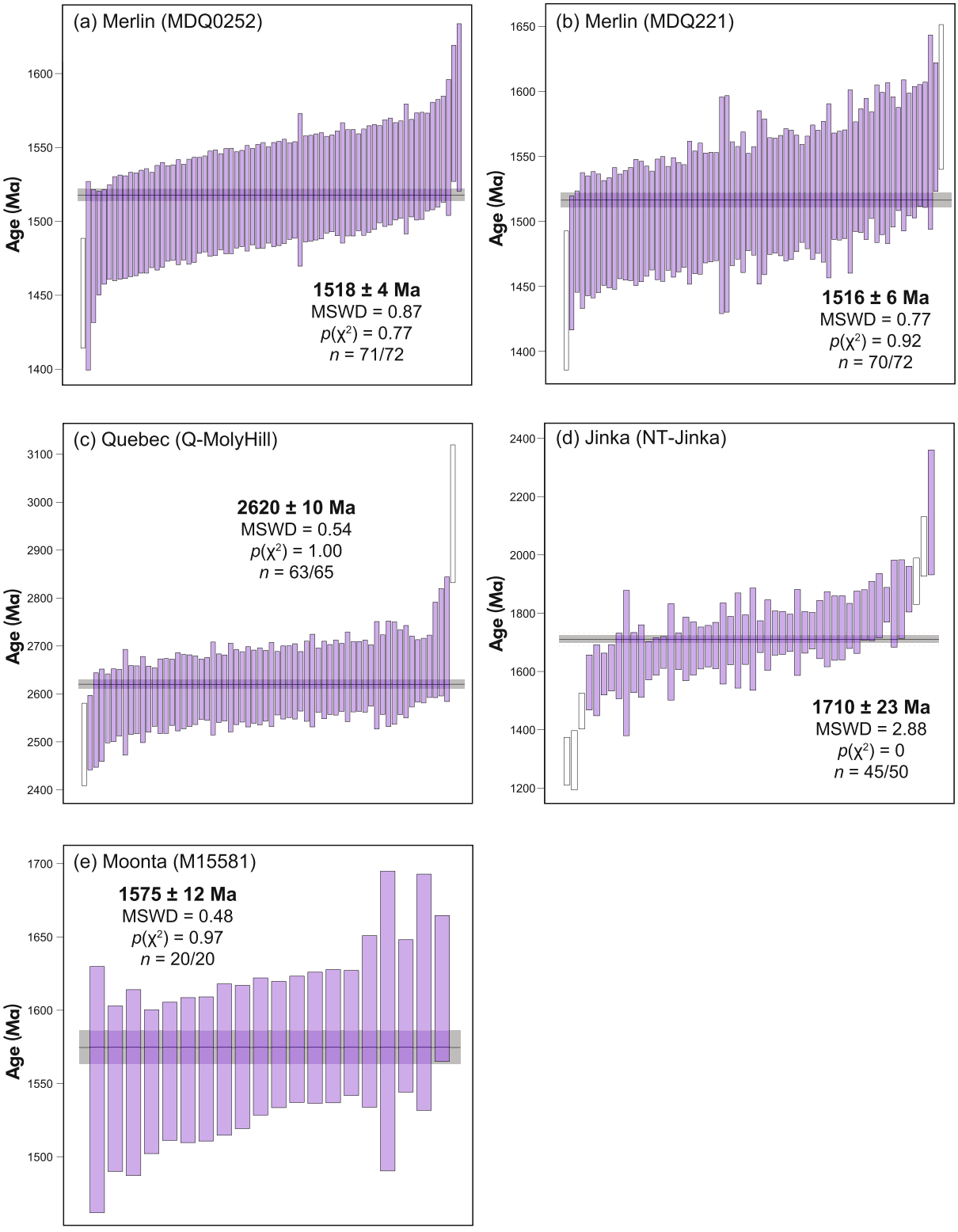

Figure 2. Results of LA-ICP-MS/MS of molybdenite. Molybdenite samples are presented as weighted means at they contain no common Os, as such individual spot ages can be calculated. Uncoloured analyses were not included in the weighted mean age calculations, as they were determined as outliers by the program IsoplotR (Vermeesch 2018). All uncertainties are 2s. (a) Sample MDQ0252, (b) Sample MDQ221, (c) Sample Q-MolyHill, (d) Sample NT-Jinka and (e) Sample M15581.

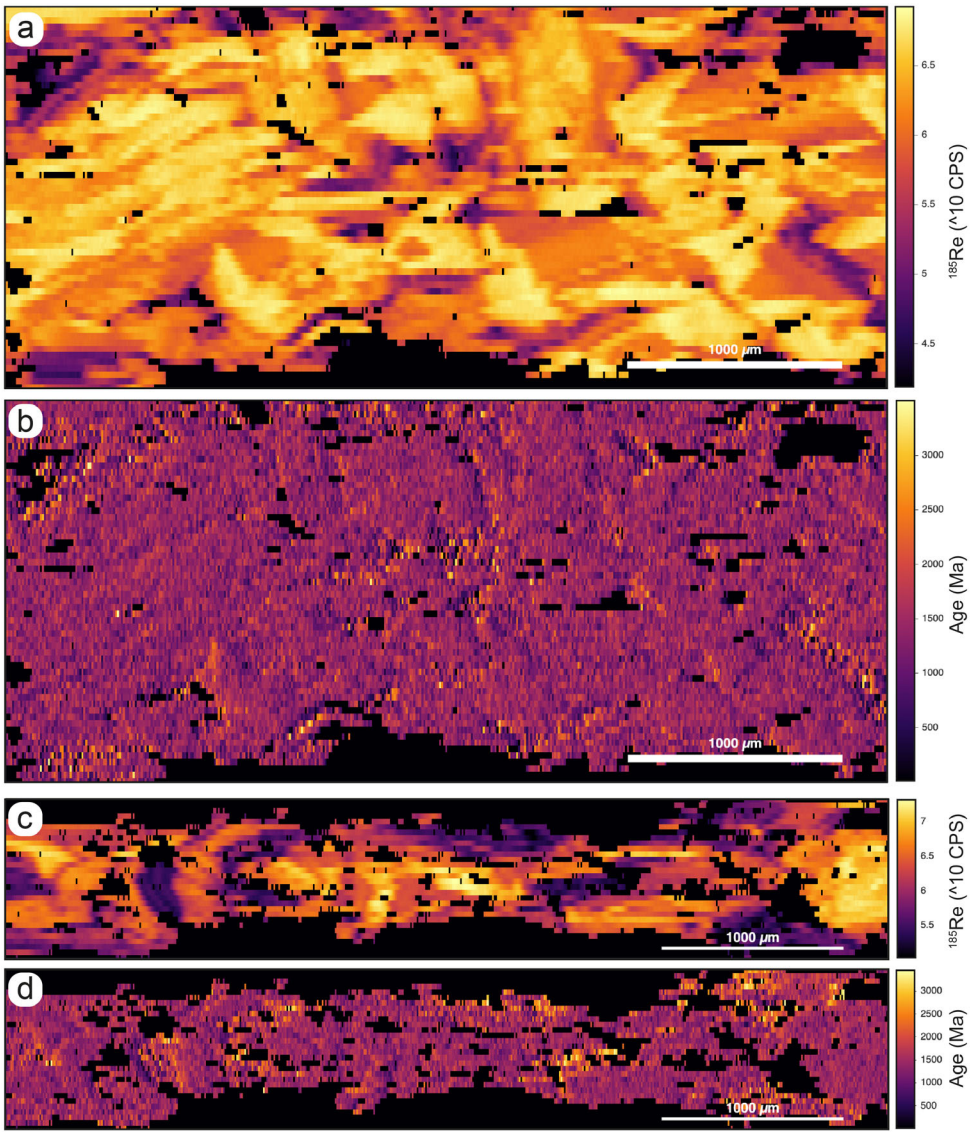

Figure 3. Results of molybdenite trace element and Re-Os age mapping. (a) Re map of MDQ0252. (b) Age map of MDQ0252. (c) Re map of MDQ0120. (d) Age map of MDQ0120.

(Figure 4d, MSWD = 3.9) can be calculated based on all five aliquots. The weighted mean of the resulting ages is 2623 ± 6 Ma, including the uncertainty on the Re decay constant (n = 5, MSWD = 1.3, Figure 4d).

Discussion

Assessment of MDQ0252 and Q-MolyHill as Re-Os reference materials

Molybdenite samples MDQ0252 from the Merlin deposit and Q-MolyHill from the Preissac pluton in Quebec were selected as candidates for reference material development. Using the Re-Os ID-TIMS ratio for MDQ0252 as the primary RM, LA-ICP-MS/MS ages obtained for Q-MolyHill are identical with the TIMS age within measurement uncertainty (Figure 5, Table 1). Hogmalm *et al.* (2019) use a mean calibration factor to calculate ages for natural molybdenite, which compares the analysed Re-Os ratios with the expected age from pressed pellets ([$^{187+14}$Os/$^{185+14}$Re]/age). Our approach involved a direct calibration of the Re-Os ratios to the MDQ0252 molybdenite crystals during data reduction, and therefore did not require an external correction factor to be applied during the calculation of LA-ICP-MS/MS ages.

The obtained ID-TIMS age for sample MDQ0252 is identical to the published age presented by Babo *et al.* (2017), suggesting it could be used as a reliable reference value. However, the results of our ID-TIMS analysis

Table 4.
Measurement results for molybdenite aliquots by ID-TIMS

Sample	Test portion mass (g)	Re (μg g^{-1})	± 2*s*	^{187}Re (ng g^{-1})	± 2*s*	^{187}Os (ng g^{-1})	± 2*s*	Total common Os present (pg)	^{187}Os/^{187}Re	± 2*s*	Age (Ma)	± 2*s*
M252m1_1	0.0566	1052.84	6.55	661752.75	4116.4	17051.1	3.57	64.64	0.0257666	0.000166	1526.29	12.93
M252m1_2	0.0621	1317.82	3.85	828309.39	2417.7	20979.42	5	114.81	0.025328	0.00008	1500.63	7.8
M252m1_3	0.0576	1192.6	3.5	749602.68	2197.2	19136.66	6.81	106.58	0.0255291	8.39E-05	1512.4	8.06
M252m1_4	0.0577	1065.89	3.09	669960.16	1940.2	17229.83	7.42	111.42	0.0257177	8.55E-05	1523.43	8.18
M252m1_5	0.0576	1043.03	3.21	655588.22	2018.8	16833.93	5.51	53.57	0.0256776	8.75E-05	1521.09	8.28
M252m1_6	0.0604	1130.29	3.41	710436.42	2142.7	18219.74	6.53	83.86	0.0256458	8.65E-05	1519.23	8.23
Q-MolyHill_1	0.0597	51.32	0.14	32254.98	88.34	1441.29	0.47	6.89	0.0446843	0.000137	2622.68	13.4
Q-MolyHill_2	0.0574	44.49	0.12	27963.78	74.32	1255.75	0.28	15.33	0.0449062	0.000129	2635.42	12.96
Q-MolyHill_3	0.0587	50.92	0.14	32005.53	89.85	1426.93	0.51	5.27	0.0445839	0.000141	2616.91	13.62
Q-MolyHill_4	0.0599	49.14	0.13	30888.13	82.6	1380.56	0.44	5.44	0.0446955	0.000134	2623.32	13.19
Q-MolyHill_5	0.0556	49.75	0.14	31269.83	90.33	1394.22	0.36	4.36	0.0445869	0.00014	2617.08	13.58

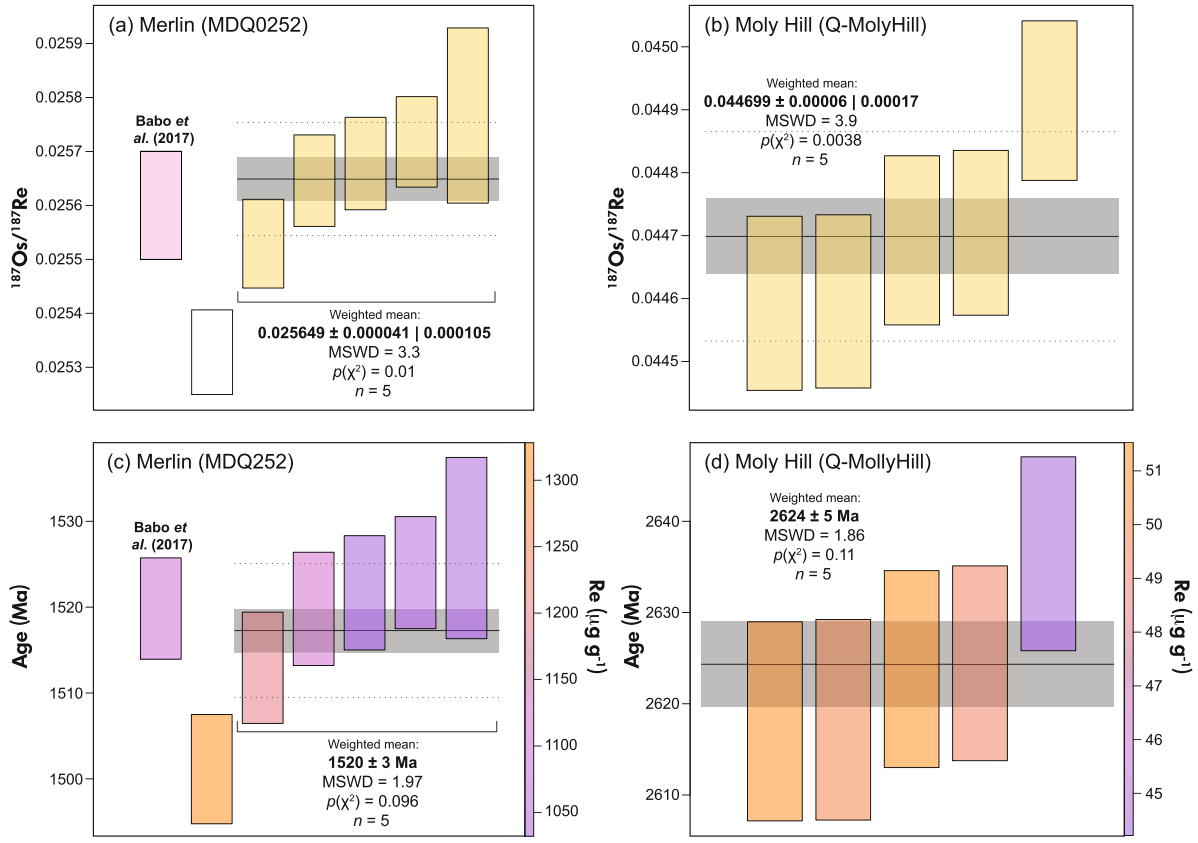

Figure 4. Plots of measurement results from ID-TIMS (all uncertainties are 2*s*). Where a second uncertainty is reported, it incorporates over dispersion in the data, due to a large MSWD, as calculated by IsoplotR (Vermeesch 2018). ^{187}Os/^{187}Re ratios and calculated ages are shown for comparison, as well as results from Babo et al. (2017). The uncoloured analysis in (a) sample MDQ0252, was determined as an outlier by IsoplotR (Vermeesch 2018). (b) contains data for sample Q-MolyHill. (c) and (d) are coloured for Re mass fraction, age uncertainties include the propagated uncertainty on the Re decay constant.

of MDQ0252 show that ^{187}Os/^{187}Re ratios from single aliquots are not homogenous, and hence form a spread in calculated ages between 1501 ± 8 to 1527 ± 13 Ma. Most data, however, produce *ca.* 1520 Ma ages (Figure 4c). The younger ages are also directly correlated with higher Re mass fractions (Figure 4c), suggesting that

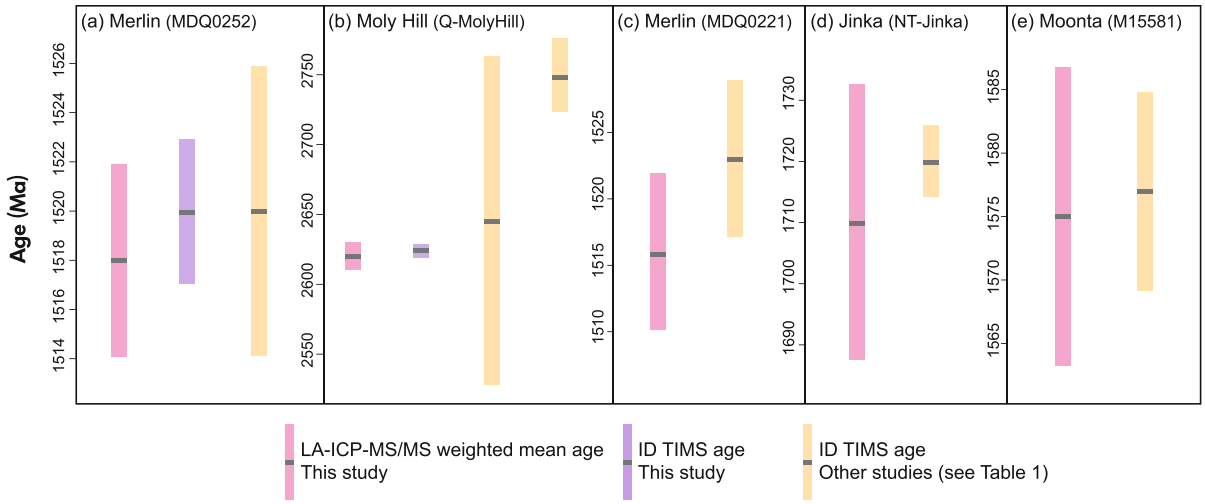

Figure 5. Summary of LA-ICP-MS/MS, ID-TIMS and literature ages from samples in this study. LA-ICP-MS/MS and ID-TIMS ages from this study are within uncertainty of each other (Table 1). (a) Sample MDQ0252, (b) Sample MDQ221, (c) Sample Q-MolyHill, (d) Sample NT-Jinka and (e) Sample M15581.

there may have been a recrystallisation or precipitation of higher-Re molybdenite at *ca.* 1500 Ma. This is consistent with molybdenite geochronology and textural interpretations of the Merlin deposit, which record the formation of minor molybdenite veins and disseminations at *ca.* 1500 Ma (Babo *et al.* 2017). While this event is interpreted to only be minor in the deposit, it appears to have had a detectable effect on the molybdenite veins from sample MDQ0252. Components of the younger *ca.* 1500 Ma ages may also be present in the LA-ICP-MS/MS data, however these are difficult to identify as the uncertainty on each individual data point is too large for such assessment (Figure 2a). We suggest, therefore, that MDQ0252 can be used as a reliable reference material for *in situ* Re-Os dating when Re mass fractions are monitored and high Re outliers are excluded. Following these recommendations, we have used MDQ0252 as the primary reference material for all LA-ICP-MS/MS analyses in this study.

The molybdenite from Moly Hill in Quebec may also be considered as a potential primary reference material for future Re-Os analysis. *In situ* LA-ICP-MS/MS analyses and ID-TIMS analyses both show that the molybdenite is homogenous in $^{187}Os/^{187}Re$ ratios and has reasonable but not excessively high Re mass fractions (between 5 and 60 $\mu g\ g^{-1}$). The latter is important as very high Re mass fractions using a large spot size can trigger the detector in the ICP-MS/MS to shift from pulse to analogue mode, which means that the analysed reference material can no longer correct for unknown analyses in pulse mode, due to difficulties in determining accurate pulse-to-analogue correction factors in the ICP-MS/MS. When sample MDQ0252 is analysed using large spot sizes ($>$ 100 µm) the Re can be measured in analogue mode, as it contains very high Re mass fractions (up to ~ 5100 $\mu g\ g^{-1}$). Importantly, the reference materials developed in this study are natural molybdenite crystals and not nano-powders. Hence, there were no matrix effects during ablation between the reference material and the unknown molybdenite samples.

Re-Os case studies

In this section, we demonstrate the reliability of the presented approach for LA-ICP-MS/MS Re-Os geochronology using case studies of several molybdenite samples with known ages (Figure 5). A second molybdenite sample from the Merlin deposit (MDQ0221) returned an *in situ* age of 1516 ± 6 Ma (n = 70, MSWD = 0.77), within uncertainty to those from a previous ID-TIMS study (1523 ± 6 Ma, Babo *et al.* 2017; Figure 5c). Molybdenite from the Jinka area in the Northern Territory also returned an *in situ* age of 1710 ± 20 Ma (n = 45, MSWD = 2.88), which is with within uncertainty of Re-Os ID-TIMS (1720 ± 9 Ma) and hornblende Ar-Ar ages (1701.6 ± 4.8 Ma) from the same deposit (Cross 2009, Reno and Fraser 2021; Figure 5), despite low Re mass fractions in the analysed grains (0.1 to 15 $\mu g\ g^{-1}$). The scatter in the individual ages, as seen in the weighted mean of the ages with an MSWD of 2.8, could be due to low Re and therefore low ^{187}Os analyses, which have low signal to noise ratios and are susceptible to scatter caused by the ^{187}Re interference correction (Figure 2d, Figure S2). The scatter could also be due to isotopic disequilibrium within the analysed molybdenite crystals.

Molybdenite from Yelta mine in the Moonta-Wallaroo district returned similar ages within uncertainty (1575 ± 12 Ma, n = 20, MSWD = 0.48) to Re-Os ID-TIMS ages from other molybdenite deposits within the area (1599 ± 6 Ma and 1574 ± 6 Ma, Skirrow *et al.* 2007; Figure 5e).

No strong evidence for significant age variation (i.e., differing extents of within-grain Re and Os mobility) between Re and Os was observed outside uncertainty in this study in molybdenite. Many studies suggesting that decoupling may create scatter in the data from microbeam methods, and that whole homogenised molybdenite grains or large fractions should only be considered for isotopic analysis (Košler *et al.* 2003, Stein *et al.* 2003, Selby and Creaser 2004, Zimmerman *et al.* 2022). However this approach is only applicable if Re or Os are not lost from the molybdenite crystal. Considering the small sampling size in each analysis and the precise spatial resolution, LA-ICP-MS/MS is the most likely method to detect microscale decoupling of Re from its daughter isotope. The NT-Jinka sample in particular may show evidence of some isotopic disequilibrium or resetting, as there are several outliers, and the weighted mean population has a high MSWD of 2.88. This may warrant further *in situ* Re-Os analyses and textural and geochemical investigation into the molybdenite from Jinka. We also note that Re and Os resetting may occur within the measurement precision of the method and therefore may not be detected. LA-ICP-MS/MS may provide a fruitful method for investigating case studies of Re and Os decoupling in the future to better understand the phenomenon, as has been done in many other geochronometers by microbeam methods.

Age mapping of two molybdenite samples from the Merlin Deposit shows the potential use of *in situ* LA-ICP-MS/MS mapping with multi-mineral calibration for correlating Re-Os ages with trace elements, to investigate age zoning or unravel the petrogenetic history of molybdenite grains (Figure 3; e.g., Markmann *et al.* 2024). Molybdenite from MDQ0252 shows similar heterogeneity in Re mass fraction as calculated from single spot analyses; with grains containing up to 5100 μg g^{-1} Re (Figure 3a). The age map contains residual measurement artefacts, generated from the sequential measurement of isotopes across grain boundaries and regions of contrasting Re mass fractions, but generally shows that the molybdenite is homogenously *ca.* 1500 Ma despite the variation in Re zoning (Figure 3b). Re-Os isotopic mapping of a molybdenite vein from another sample from the Merlin deposit (MDQ0120) shows potential variable age zoning (Figure 3b). Grains or domains of the molybdenite with high Re mass fractions (up to 1600 μg g^{-1}) are correlated with low Cu, Ni and Ag and generally are inversely correlated with the Re-Os ages (Figure S1). Based on these two examples, simultaneous Re-Os age and trace element mapping using the *in situ* method seems promising and may be a useful future application, especially in mineral systems with complex multi-stage histories.

Strengths and limitations of the Re-Os LA-ICP-MS/MS method

The relationship between Re mass fraction, corresponding radiogenic ^{187}Os mass fraction, age, and single spot or weighted mean age uncertainty is presented in Figure 6. The lowest uncertainty obtained on individual analyses in this study is ~ 3% (Figure 6b). However, all calculated weighted mean ages for molybdenite analysed by the LA-ICP-MS/MS method return age uncertainties under 1.4% (n = 20–70), even for low Re samples (< 10 μg g^{-1}, Table 1, Figure 5). The precise *in situ* Re-Os ages can be explained by the age-homogenous nature of the molybdenite grains analysed, forming single age populations (Figure 2), and the absence of common Os in any analyses. The limits on age or Re mass fractions to produce useful dates using the applied method are difficult to constrain, as the detection limit of $^{187+14}Os$ is difficult to estimate due to the lack of a primary reference material with a homogenous Os mass fraction, and will depend on the spot size utilised during ablation. The median $^{187+14}Re$ detection limit across the three measurement sessions is ~ 0.005 μg g^{-1}, considering the lower isotopic abundance and higher ionisation potential of $^{187+14}Os$, the detection limit of $^{187+14}Os$ is probably much higher than this value. However, the lowest $^{187+14}Os$ detectable by this technique may still have large uncertainties due to low signal to noise ratios, and therefore analyses may still be imprecise. For ^{187}Os mass fractions between ~ 0.5 and 0.1 μg g^{-1}, uncertainties on individual analyses increase to over 5%, although weighted mean ages calculated from this sample are still only 1.4% (Figure 6).

The molybdenite dataset of Barton *et al.* (2020) contains average Re values and ages for 3089 molybdenite samples from over 700 ore-bearing hydrothermal systems. Calculation of ^{187}Os from this database allows us to estimate the proportion of molybdenite that may return meaningful ages using the *in situ* method. If a very conservative 'minimum ^{187}Os' mass fraction required to calculate a precise weighted mean age (< 1.4%) of ~ 0.01 μg g^{-1} is considered, then 81% of molybdenite in the database could produce precise Re-Os ages using the *in situ* method, provided the data are not over dispersed (Figure 6). However, we note that the database may be biased to higher-Re samples, due to sampling bias and by

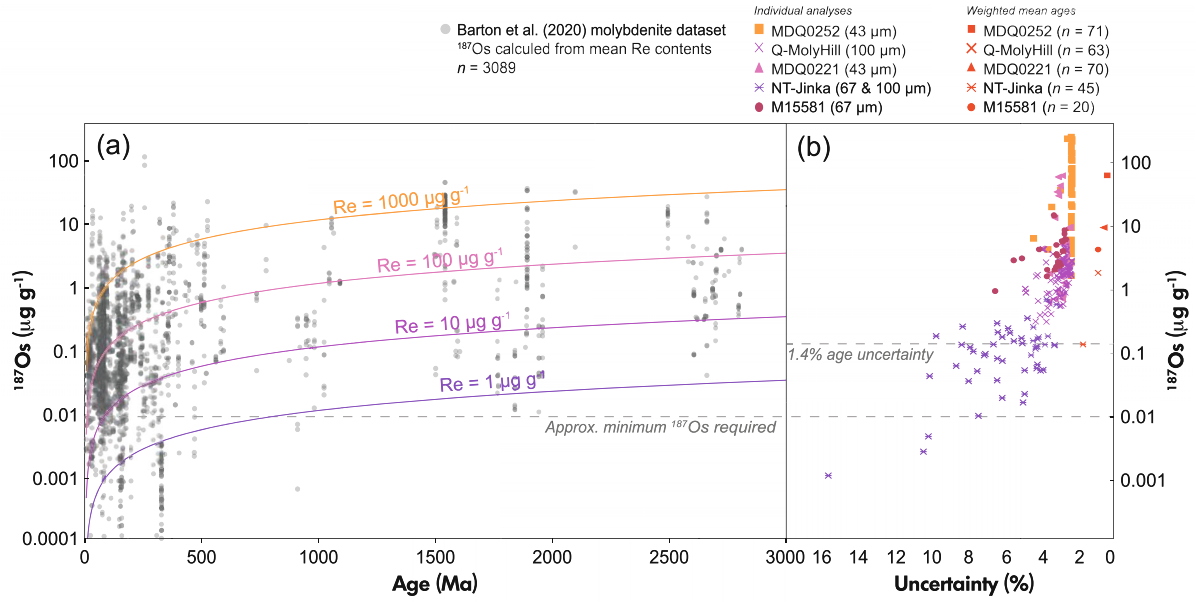

Figure 6. (a) Relationship between Re mass fraction, radiogenic ^{187}Os mass fraction, age, and (b) individual (spot) measurement uncertainty (2*s*, including propagated uncertainty on the decay constant of ^{187}Re) and weighted mean age uncertainty. The ^{187}Os mass fraction of the weighted mean ages is an average. For low Re and therefore low radiogenic ^{187}Os molybdenite, individual measurement uncertainties become significant (> 5%). However, when low Re and therefore low radiogenic ^{187}Os (e.g., NT-Jinka) data is pooled in weighted means, the uncertainties on calculated ages are still excellent. For comparison, ^{187}Os mass fractions are calculated from Re content and age from the molybdenite database of Barton *et al.* (2020). Note that these estimations are relevant for samples with no common Os.

the detection limit for Re from the analytical technique utilised. Nevertheless, low Re (< 10 µg g^{-1}) molybdenite of Precambrian age may still produce precise and accurate *in situ* Re-Os weighted mean ages. A limitation of this method is recognised for young ages (< 150 Ma), where low Re (< ~ 20 ppm) samples may not be able to provide precise ages via this technique. For a full discussion of Re contents in molybdenite in different style of deposits, the reader is referred to Barton *et al.* (2020).

Another potential limitation of the *in situ* method is the inability to resolve temporally similar age populations within samples. The significant uncertainties on individual analyses may not allow separate age populations to be discerned without textural or compositional evidence. For example, ID-TIMS analysis suggests that Merlin sample MDQ0252 records two molybdenite crystallisation events, at *ca.* 1520 and 1500 Ma (Figure 4). We did not see significant scatter in our *in situ* measurements of Merlin sample MDQ0252, which would suggest that we analysed these two age populations. If molybdenite age populations are within ~ 3% of each other in other samples, this detail may not be statistically resolvable using the LA-ICP-MS/MS method. However, with other lines of evidence, such as those obtained from textural or compositional (i.e., trace element) analysis, it may be possible to discern multiple ages in *in situ* molybdenite analyses.

Strengths of this technique include the ability to target specific molybdenite grains and textures *in situ*, as well as to collect trace element data simultaneously to determine the composition and to assist in understanding the petrogenesis of the analysed sulfides. The *in situ* approach also provides an opportunity to remove measurement intervals of inclusions in time-resolved LA-ICP-MS/MS data, ensuring that only the target mineral is incorporated into Re-Os isotopic calculations. Small grains (30 µm) can be analysed in this method, allowing for analysis of fine grained or dispersed molybdenite, which may not be feasible to analyse using traditional methods. Additionally, simultaneous age and trace element mapping may provide significant advances in our understanding of molybdenite growth and/or Re and Os isotopic disequilibrium (e.g., Figure 3, Figure S1). Future avenues of method development may include the investigation of Re and Os decoupling within molybdenite grains and Re or Os nanoparticle formation (Barra *et al.* 2017), trace element and age mapping of molybdenite, and the

dating of Re-poor minerals such as pyrite, chalcopyrite and cobaltite (e.g., Saintilan *et al.* 2017, Li *et al.* 2022).

Among the most important advantages of the *in situ* approach are the relatively simple sample preparation requirements and the rapid and cost effective data acquisition. These aspects, together with the high spatial resolution, open opportunities to efficiently complete large geochronology campaigns on ore systems that very commonly have complex multi-stage mineralisation events, such as Precambrian ore deposits where protracted geological histories are common (e.g., Haroldson *et al.* 2020, Schutesky and de Oliveira 2020, Maas *et al.* 2022). The methodology offers additional benefits to the minerals industry where rapid acquisition of geochronological data on ore formation is needed to influence investment decisions on exploration and resource development.

Conclusions

In situ LA-ICP-MS/MS measurement of Re-Os provides accurate and precise age data for molybdenite. Two natural molybdenites, MDQ0252 from the Merlin deposit in Queensland and Q-MolyHill from the Preissac pluton in Quebec, have been developed as potential reference materials for *in situ* analysis. These samples contain homogenous Re-Os isotope ratios and have Re mass fractions amenable to LA-ICP-MS/MS analysis. The spatial resolution afforded by the *in situ* approach allows targeting of textural domains, growth zones, and small or scare grains. Additional benefits include the simple sample preparation, rapid and cost effective data acquisition and capability for simultaneous collection of trace elements, all of which facilitate improved understanding of the timing and nature of ore-forming or fluid events in sulfide-bearing systems. Other future directions include the ability to trace element and age map sulfides, to provide a possible avenue to investigate age and trace element variability in individual sulfides, as well as the opportunity to investigate Re and Os isotopic disequilibrium in molybdenite.

Acknowledgements

We would like to thank Adelaide Microscopy for their support of this project, including Aoife McFadden and Ben Wade for analytical assistance. Barry Reno of the Geological Survey of the Northern Territory is thanked for supplying sample NT-Jinka. We also thank Mitchell Bockmann (Geological Survey of South Australia) and Anthony Milnes (Tate Memorial Museum) for discussions and for supplying sample materials. We thank Mike Gadd from the Geological Survey of Canada for excellent discussions and comments on this manuscript. Christopher Lawley from the Geological Survey of Canada and Balz Kamber are also acknowledged for comments on an earlier version of this work. Two anonymous reviewers are thanked for their comments, and Regina Mertz-Kraus is thanked for editorial handling. The work was supported by the Mineral Exploration Cooperative Research Centre whose activities are funded by the Australian Government's Cooperative Research Centre Programme. This is MinEx CRCocument 2024/06. S. Glorie and C. Spandler were supported by funding from the Australian Research Council (FT210100906 and LP190100635, respectively). The authors declare no conflicts of interest related to this publication. Open access publishing facilitated by The University of Adelaide, as part of the Wiley - The University of Adelaide agreement via the Council of Australian University Librarians.

Scientific editing by Regina Mertz-Kraus.

Data availability statement

LA-ICP-MS/MS and ID-TIMS data are available in the online supporting information; further data and reference materials are available upon request to the corresponding author.

References

Babo J., Spandler C., Oliver N.H.S., Brown M., Rubenach M.J. and Creaser R.A. (2017)
The high-grade Mo-Re Merlin deposit, Cloncurry district, Australia: Paragenesis and geochronology of hydrothermal alteration and ore formation. **Economic Geology, 112**, 397–422.

Barra F., Deditius A., Reich M., Kilburn M.R., Guagliardo P. and Roberts M.P. (2017)
Dissecting the Re-Os molybdenite geochronometer. **Scientific Reports, 7**, 1–7.

Barra F., Ruiz J., Valencia V.A., Ochoa-Landín L., Chesley J.T. and Zurcher L. (2005)
Laramide porphyry Cu-Mo mineralization in northern Mexico: Age constraints from Re-Os geochronology in molybdenite. **Economic Geology, 100**, 1605–1616.

Barraclough E. (1979)
Geological investigations at the Molyhill scheelite mine, central Australia. **NT Geological Survey GS 79**, 11–53.

Barton I.F., Rathkopf C.A. and Barton M.D. (2020)
Rhenium in molybdenite: A database approach to identifying geochemical controls on the distribution of a critical element. **Mining, Metallurgy and Exploration, 37**, 21–37.

Bingen B. and Stein H. (2003)
Molybdenite Re-Os dating of biotite dehydration melting in the Rogaland high-temperature granulites, S Norway. **Earth and Planetary Science Letters, 208**, 181–195.

references

Birck J-L., Roy Barman M. and Capmas F. (1997)
Re-Os isotopic measurements at the femtomole level in natural samples. **Geostandards Newsletter: The Journal of Geostandards and Geoanalysis**, **21**, 19–27.

Bockmann M.J., Hand M., Morrissey L.J., Payne J.L., Hasterok D., Teale G. and Conor C. (2022)
Punctuated geochronology within a sustained high-temperature thermal regime in the southeastern Gawler Craton. **Lithos**, **430**, 106860.

Brown M., Lazo F., Carter P., Goss B. and Kirwin D. (2010)
The geology and discovery of the Merlin Mo-Re zone of the Mount Dore deposit, Mount Isa Inlier, NW Queensland, Australia. **SGA News**, **27**, 9–15.

Chen J.H., Papanastassiou D.A. and Wasserburg G.J. (2002)
Re-Os and Pd-Ag systematics in group IIIAB irons and in pallasites. **Geochimica et Cosmochimica Acta**, **66**, 3793–3810.

Ciobanu C.L., Cook N.J., Kelson C.R., Guerin R., Kalleske N. and Danyushevsky L. (2013)
Trace element heterogeneity in molybdenite fingerprints stages of mineralization. **Chemical Geology**, **347**, 175–189.

Cohen A.S. and Waters F.G. (1996)
Separation of osmium from geological materials by solvent extraction for analysis by thermal ionisation mass spectrometry. **Analytica Chimica Acta**, **332**, 269–275.

Danyushevsky L., Robinson P., Gilbert S., Norman M., Large R., McGoldrick P. and Shelley M. (2011)
Routine quantitative multi-element analysis of sulphide minerals by laser ablation ICP-MS: Standard development and consideration of matrix effects. **Geochemistry: Exploration, Environment, Analysis**, **11**, 51–60.

Ducharme Y., Stevenson R.K. and Machado N. (1997)
Sm-Nd geochemistry and U-Pb geochronology of the Preissac and Lamotte leucogranites, Abitibi Subprovince. **Canadian Journal of Earth Sciences**, **34**, 1059–1071.

Feely M., Costanzo A., Gaynor S.P., Selby D. and McNulty E. (2020)
A review of molybdenite, and fluorite mineralisation in Caledonian granite basement, western Ireland, incorporating new field and fluid inclusion studies, and Re-Os and U-Pb geochronology. **Lithos**, **354**, 105267.

Fraser T.A. and Hutchison M.P. (2017)
Lithogeochemical characterization of the Middle–Upper Devonian Road River Group and Canol and Imperial Formations on Trail River, east Richardson Mountains, Yukon: Age constraints and a depositional model for fine-grained strata in the Lower Paleozoic Richardson Trough. **Canadian Journal of Earth Sciences**, **54**, 731–765.

Gilbert S.E. and Glorie S. (2020)
Removal of Hg interferences for common Pb correction when dating apatite and titanite by LA-ICP-MS/MS. **Journal of Analytical Atomic Spectrometry**, **35**, 1472–1481.

Gilbert S., Danyushevsky L., Robinson P., Wohlgemuth-Ueberwasser C., Pearson N., Savard D., Norman M. and Hanley J. (2013)
A comparative study of five reference materials and the Lombard meteorite for the determination of the platinum-group elements and gold by LA-ICP-MS. **Geostandards and Geoanalytical Research**, **37**, 51–64.

Guillong M. and Günther D. (2002)
Effect of particle size distribution on ICP-induced elemental fractionation in laser ablation-inductively coupled plasma-mass spectrometry. **Journal of Analytical Atomic Spectrometry**, **17**, 831–837.

Håkansson I. (2019)
In situ Re-Os dating of molybdenite using LA-ICP-MS/MS – Analytical protocol and standardization. **BSc Thesis, University of Gothenburg**, 35pp.

Haroldson E.L., Brown P.E., Ishida A. and Valley J.W. (2020)
SIMS oxygen isotopes indicate Phanerozoic fluids permeated a Precambrian gold deposit. **Chemical Geology**, **533**, 119429.

Hirt B. (1963)
Age determination by the rhenium-osmium method. **International Atomic Energy Agency, Radioactive Dating**, 35–44.

Hnatyshin D., Creaser R.A., Meffre S., Stern R.A., Wilkinson J.J. and Turner E.C. (2020)
Understanding the microscale spatial distribution and mineralogical residency of Re in pyrite: Examples from carbonate-hosted Zn-Pb ores and implications for pyrite Re-Os geochronology. **Chemical Geology**, **533**, 119427.

Hogmalm K.J., Dahlgren I., Fridolfsson I. and Zack T. (2019)
First *in situ* Re-Os dating of molybdenite by LA-ICP-MS/MS. **Mineralium Deposita**, **54**, 821–828.

Hou Z., Zeng P., Gao Y., Du A. and Fu D. (2006)
Himalayan Cu-Mo-Au mineralization in the eastern Indo-Asian collision zone: Constraints from Re-Os dating of molybdenite. **Mineralium Deposita**, **41**, 33–45.

Huang X-W., Gao J-F., Qi L. and Zhou M-F. (2015)
In situ LA-ICP-MS trace elemental analyses of magnetite and Re-Os dating of pyrite: The Tianhu hydrothermally remobilized sedimentary Fe deposit, NW China. **Ore Geology Reviews**, **65**, 900–916.

Huminicki M.A.E (2005)
Quantitative mass balance of platinum-group elements in the Kelly Lake Ni-Cu-PGE deposit, Copper Cliff Offset, Sudbury. **Economic Geology**, **100**, 1631–1646.

references

Hurtig N.C., Georgiev S.V, Zimmerman A., Yang G., Goswami V., Hannah J.L. and Stein H.J. (2020)
Re-Os geochronology for the NIST RM 8505 crude oil: The importance of analytical protocol and uncertainty. Chemical Geology, 539, 119381.

Huston D.L., Norman M., Maas R., Miggins D., Thiede D.S., Vasconcelos P., Creaser R., Cross A.J., Bennett V., Bottrill R., Lisitsin V., Duncan R., Forster D., Brauhart C., Dhnaram C., Champion D., Czarnota K. and Whitaker A. (2022)
Geochronological studies of selected Australian mineral deposits, 2003–2020. Record 2022/11.

Jochum K.P., Nohl U., Herwig K., Lammel E., Stoll B. and Hofmann A.W. (2005)
GeoReM: A new geochemical database for reference materials and isotopic standards. Geostandards and Geoanalytical Research, 29, 333–338.

Kositcin N., McGloin M.V., Reno B.L., Weisheit A. and Beyer E.E. (2018)
Summary of Results. Joint NTGS-GA geochronology project: Base metal and tungsten mineralisation, and skarn alteration in the Aileron Province July 2017–June 2018. Northern Territory Geological Survey, NTGS Record 2018-009, 30pp.

Košler J., Simonetti A., Sylvester P.J., Cox R.A., Tubrett M.N. and Wilton D.H.C. (2003)
Laser-ablation ICP-MS measurements of Re/Os in molybdenite and implications for Re-Os geochronology. The Canadian Mineralogist, 41, 307–320.

Kuhn H-R. and Günther D. (2004)
Laser ablation-ICP-MS: Particle size dependent elemental composition studies on filter-collected and online measured aerosols from glass. Journal of Analytical Atomic Spectrometry, 19, 1158–1164.

Li W., Jin X., Gao B., Zhou L., Yang G., Li C., Stein H., Hannah J., Du A. and Qu W. (2022)
Chalcopyrite from the Xiaotongchang Cu deposit: A new sulfide reference material for low-level Re-Os geochronology. Geostandards and Geoanalytical Research, 46, 321–332.

Li Y. and Vermeesch P. (2021)
Inverse isochron regression for Re-Os, K-Ca and other chronometers. Geochronology, 3, 415–420.

Maas R., Apukhtina O.B., Kamenetsky V.S., Ehrig K., Sprung P. and Muenker C. (2022)
Carbonates at the supergiant Olympic dam Cu-U-Au-Ag deposit, South Australia Part 2: Sm-Nd, Lu-Hf and Sr-Pb isotope constraints on the chronology of carbonate deposition. Ore Geology Reviews, 140, 103745.

Markey R., Stein H.J., Hannah J.L., Zimmerman A., Selby D. and Creaser R.A. (2007)
Standardizing Re-Os geochronology: A new molybdenite reference material (Henderson, USA) and the stoichiometry of Os salts. Chemical Geology, 244, 74–87.

Markey R., Stein H. and Morgan J. (1998)
Highly precise Re-Os dating for molybdenite using alkaline fusion and NTIMS. Talanta, 45, 935–946.

Markmann T.A., Lanari P., Piccoli F., Pettke T., Tamblyn R., Tedeschi M., Lueder M., Kunz B.E., Riel N. and Laughton J. (2024)
Multi-phase quantitative compositional mapping by LA-ICP-MS: Analytical approach and data reduction protocol implemented in XMapTools. Chemical Geology, 646, 121895.

Meibom A. and Frei R. (2002)
Evidence for an ancient osmium isotopic reservoir in Earth. Science, 296, 516–518.

Meisel T., Walker R.J., Irving A.J. and Lorand J-P. (2001)
Osmium isotopic compositions of mantle xenoliths: A global perspective. Geochimica et Cosmochimica Acta, 65, 1311–1323.

Morrow D.W. (1999)
Lower Paleozoic stratigraphy of northern Yukon Territory and northwestern district of Mackenzie. Geological Survey of Canada Bulletin, 538, 202pp.

Norris A. and Danyushevsky L. (2018)
Towards estimating the complete uncertainty budget of quantified results measured by LA-ICP-MS. Goldschmidt Conference (Boston, MA, USA).

Pašava J., Svojtka M., Veselovský F., Ďurišová J., Ackerman L., Pour O., Drábek M., Halodová P. and Haluzová E. (2016)
Laser ablation ICP-MS study of trace element chemistry in molybdenite coupled with scanning electron microscopy (SEM) – An important tool for identification of different types of mineralization. Ore Geology Reviews, 72, 874–895.

Paton C., Hellstrom J., Paul B., Woodhead J. and Hergt J. (2011)
Iolite: Freeware for the visualisation and processing of mass spectrometric data. Journal of Analytical Atomic Spectrometry, 26, 2508–2518.

Ravizza G. and Turekian K.K. (1992)
The osmium isotopic composition of organic-rich marine sediments. Earth and Planetary Science Letters, 110, 1–6.

Redaa A., Farkaš J., Gilbert S., Collins A.S., Wade B., Löhr S., Zack T. and Garbe-Schönberg D. (2021)
Assessment of elemental fractionation and matrix effects during *in situ* Rb-Sr dating of phlogopite by LA-ICP-MS/MS: Implications for the accuracy and precision of mineral ages. Journal of Analytical Atomic Spectrometry, 36, 322–344.

Reid A., Smith R.N., Baker T., Jagodzinski E.A., Selby D., Gregory C.J. and Skirrow R.G. (2013)
Re-Os dating of molybdenite within hematite breccias from the Vulcan Cu-Au prospect, Olympic Cu-Au province, South Australia. Economic Geology, 108, 883–894.

Reisberg L., France-Lanord C. and Pierson-Wickmann A-C. (1997)
Os isotopic compositions of leachates and bulk sediments from the Bengal Fan. Earth and Planetary Science Letters, 150, 117–127.

Reno B.L. and Fraser G.L. (2021)
Summary of results. Joint NTGS-GA geochronology project: Constraining cooling and deformation in the eastern Aileron Province through $^{40}Ar/^{39}Ar$ step-heating of hornblende, muscovite and biotite. NTGS Record 2022-001, 89pp.

references

Roberts N.M.W., Rasbury E.T., Parrish R.R., Smith C.J., Horstwood M.S.A. and Condon D.J. (2017)
A calcite reference material for LA-ICP-MS U-Pb geochronology. **Geochemistry, Geophysics, Geosystems**, 18, 2807–2814.

Ruano S.M., Both R.A. and Golding S.D. (2002)
A fluid inclusion and stable isotope study of the Moonta copper-gold deposits, South Australia: Evidence for fluid immiscibility in a magmatic hydrothermal system. **Chemical Geology**, 192, 211–226.

Sabina A.P (2003)
Rocks and minerals for the collector: Kirkland Lake-Rouyn-Noranda-Val-d'Or, Ontario and Quebec. **Geological Survey of Canada, Miscellaneous Report 77**, 322pp.

Sai Y., Jin K., Luo M., Tian H., Li J. and Liu J. (2020)
Recent progress on the research of Re-Os geochronology and Re-Os elemental and isotopic systematics in petroleum systems. **Journal of Natural Gas Geoscience**, 5, 355–365.

Saintilan N.J., Creaser R.A. and Bookstrom A.A. (2017)
Re-Os systematics and geochemistry of cobaltite (CoAsS) in the Idaho Cobalt Belt, Belt-Purcell Basin, USA: Evidence for Middle Mesoproterozoic sediment-hosted Co-Cu sulfide mineralization with Grenvillian and Cretaceous remobilization. **Ore Geology Reviews**, 86, 509–525.

Schutesky M.E. and Gouveia de Oliveira C. (2020)
From the roots to the roof: An integrated model for the Neoarchean Carajás IOCG System, Brazil. **Ore Geology Reviews**, 127, 103833.

Selby D. and Creaser R.A. (2003)
Re-Os geochronology of organic rich sediments: An evaluation of organic matter analysis methods. **Chemical Geology**, 200, 225–240.

Selby D. and Creaser R.A (2001)
Re-Os geochronology and systematics in molybdenite from the Endako Porphyry molybdenum deposit, British Columbia, Canada. **Economic Geology**, 96, 197–204.

Selby D. and Creaser R.A. (2001)
Late and mid-Cretaceous mineralization in the northern Canadian Cordillera: Constraints from Re-Os molybdenite dates. **Economic Geology**, 96, 1461–1467.

Selby D. and Creaser R.A. (2004)
Macroscale NTIMS and microscale LA-MC-ICP-MS Re-Os isotopic analysis of molybdenite: Testing spatial restrictions for reliable Re-Os age determinations, and implications for the decoupling of Re and Os within molybdenite. **Geochimica et Cosmochimica Acta**, 68, 3897–3908.

Selby D., Creaser R.A., Stein H.J., Markey R.J. and Hannah J.L. (2007)
Assessment of the ^{187}Re decay constant by cross calibration of Re-Os molybdenite and U-Pb zircon chronometers in magmatic ore systems. **Geochimica et Cosmochimica Acta**, 71, 1999–2013.

Shirey S.B. and Walker R.J. (1995)
Carius tube digestion for low-blank rhenium-osmium analysis. **Analytical Chemistry**, 67, 2136–2141.

Skirrow R.G., Bastrakov E.N., Barovich K., Fraser G.L., Creaser R.A., Fanning C.M., Raymond O.L. and Davidson G.J. (2007)
Timing of iron oxide Cu-Au-(U) hydrothermal activity and Nd isotope constraints on metal sources in the Gawler Craton, South Australia. **Economic Geology**, 102, 1441–1470.

Stein H.J., Markey R.J., Morgan J.W., Du A. and Sun Y. (1997)
Highly precise and accurate Re-Os ages for molybdenite from the east Qinling Molybdenum Belt, Shaanxi Province, China. **Economic Geology**, 92, 827–835.

Stein H.J., Markey R.J., Morgan J.W., Hannah J.L. and Scherstén A. (2001)
The remarkable Re-Os chronometer in molybdenite: How and why it works. **Terra Nova**, 13, 479–486.

Stein H.J., Sundblad K., Markey R.J., Morgan J.W. and Motuza G. (1998)
Re-Os Ages for Archean molybdenite and pyrite, Kuittila-Kivisuo, Finland and Proterozoic molybdenite, Kabeliai, Lithuania: Testing the chronometer in a metamorphic and metasomatic setting. **Mineralium Deposita**, 33, 329–345.

Stein H., Scherstén A., Hannah J. and Markey R. (2003)
Subgrain-scale decoupling of Re and ^{187}Os and assessment of laser ablation ICP-MS spot dating in molybdenite. **Geochimica et Cosmochimica Acta**, 67, 3673–3686.

Strauss J.V., Fraser T., Melchin M.J., Allen T.J., Malinowski J., Feng X., Taylor J.F., Day J., Gill B.C. and Sperling E.A. (2020)
The Road River Group of northern Yukon, Canada: Early Paleozoic deep-water sedimentation within the Great American Carbonate Bank. **Canadian Journal of Earth Sciences**, 57, 1193–1219.

Suzuki K., Shimizu H. and Masuda A. (1993)
Reliable Re-Os age for molybdenite. **Geochimica et Cosmochimica Acta**, 57, 1625–1628.

Tamblyn R., Hand M., Simpson A., Gilbert S., Wade B. and Glorie S. (2022)
In situ laser ablation Lu-Hf geochronology of garnet across the Western Gneiss Region: Campaign-style dating of metamorphism. **Journal of the Geological Society of London**, 179, 2021-94.

Wohlgemuth-Ueberwasser C.C., Ballhaus C., Berndt J., Stotter née Paliulionyte V. and Meisel T. (2007)
Synthesis of PGE sulfide standards for laser ablation inductively coupled plasma-mass spectrometry (LA-ICP-MS). **Contributions to Mineralogy and Petrology**, 154, 607–617.

Xiang D., Zhang Z., Zack T., Chew D., Yang Y., Wu L. and Hogmalm J. (2021)
Apatite U-Pb dating with common Pb correction using LA-ICP-MS/MS. **Geostandards and Geoanalytical Research**, 45, 621–642.

references

Zack T. and Hogmalm K.J. (2016)
Laser ablation Rb/Sr dating by online chemical separation of Rb and Sr in an oxygen-filled reaction cell. **Chemical Geology, 437**, 120–33.

Zimmerman A., Yang G., Stein H.J. and Hannah J.L. (2022)
A critical review of molybdenite ^{187}Re parent-^{187}Os daughter intra-crystalline decoupling in light of recent *in situ* micro-scale observations. **Geostandards and Geoanalytical Research, 46**, 761–772.

Supporting information

The following supporting information may be found in the online version of this article:

Figure S1. Trace element maps processed in Iolite (Paton *et al.* 2011) for molybdenite sample MDQ0120.

Figure S2. Rhenium reaction rates between the three measurement sessions, calculated from raw counts per second (cps) for all analysed samples and reference materials.

Table S1. *In situ* Re-Os LA-ICP-MS/MS data for reference materials (NIST SRM 610 and STDGL-3) and unknowns (samples), including corrected isotopic ratios and elemental mass fractions, and background-subtracted uncorrected cps data.

This material is available from: http://onlinelibrary.wiley.com/doi/10.1111/ggr.12550/abstract (This link will take you to the article abstract).